ChemComm

Cite this: *Chem. Commun.*, 2011, **47**, 7680–7682

www.rsc.org/chemcomm

COMMUNICATION

Facile fabrication of noble metal nanoparticles encapsulated in hollow silica with radially oriented mesopores: multiple roles of the *N*-lauroylsarcosine sodium surfactant†

Hu Wang, Jin-Gui Wang, Hui-Jing Zhou, Yu-Ping Liu, Ping-Chuan Sun and Tie-Hong Chen*

Received 13th May 2011, Accepted 24th May 2011
DOI: 10.1039/c1cc12823j

A facile one-pot method was reported to fabricate noble metal nanoparticles encapsulated in silica hollow nanospheres with radially oriented mesopores, and the anionic amino acid surfactant, *N*-lauroylsarcosine sodium, played multiple roles: reducing agent, stabilizer, emulsion droplets and mesopore template.

Metal nanoparticles have attracted broad interest in recent years because of their unique properties and potential applications in catalysis, biodetection, optics, photonics and electronics. The chemical synthesis of metal nanoparticles generally involves the reduction of metal ions by reducing agents such as hydrazine, sodium borohydride and alcohols, which are highly reactive but would have potential environmental and biological problems. For the green synthesis of metal nanoparticles, green solvent medium, an environmentally benign reducing agent and the nontoxic stabilizers of the nanoparticles are required.[1]

Metal nanoparticles encapsulated in hollow spheres, or the so called yolk–shell or rattle type particles, have attracted more and more attention.[2–5] The nanorattle structures exhibited unique optical and electrical properties and were advantageous in the fields of drug delivery and catalysts.[6–9] A variety of methods have been developed to fabricate rattle type structures, including template-assisted etching approach,[2,3,10] selectively core-etching,[5,11] the surface-protected etching process,[12] Kirkendall effect[13] or Ostwald ripening processes,[8] vesicle-based method[14] and water-in-oil microemulsion method.[15] Although progress on the synthesis of rattle type particles has been achieved, there are disadvantages in some methods, such as tedious procedures and employment of toxic and volatile organic solvents. In this work, the amino acid anionic surfactant *N*-lauroylsarcosine sodium (Sar-Na) was used as both a green reductant and stabilizer to synthesize noble metal nanoparticles in aqueous solution. Furthermore, based on the acid emulsification and templating effects of the Sar-Na, a facile one-pot method to fabricate noble metal nanoparticles encapsulated in a mesoporous hollow silica shell was also presented.

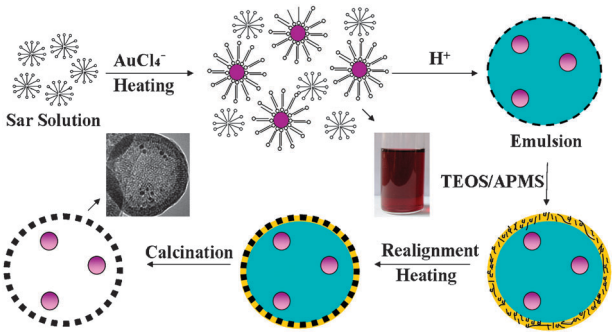

Scheme 1 Fabrication procedure of the Au@MSHS structure.

The anionic amino acid surfactant, Sar-Na (Fig. S1, ESI†), is commercially available and is commonly used in cosmetic and pharmaceutical industries due to its biodegradability and low toxicity. As shown in Scheme 1, when the solution containing Sar-Na and $AuCl_4^-$ was stirred at 353 K for 1 h (for the detailed experimental process see ESI†), the color of the solution changed from bright yellow to purple (Fig. 1), implying that Au nanoparticles were formed and suspended in the solution. The average size of Au nanoparticles was 7.9 nm (with a standard deviation of 2.6 nm) as shown in TEM images (Fig. S2, ESI†).

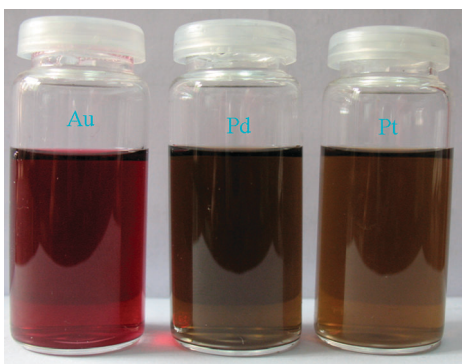

Fig. 1 Photographs of Au, Pd and Pt nanoparticles in Sar-Na solution.

Institute of New Catalytic Materials Science, Key Laboratory of Advanced Energy Materials Chemistry (MOE), College of Chemistry, Nankai University, Tianjin 300071, P. R. China. E-mail: chenth@nankai.edu.cn
† Electronic supplementary information (ESI) available. See DOI: 10.1039/c1cc12823j

As there was no other reducing agent used, it was concluded that the surfactant Sar-Na acted as a reducing agent of the Au nanoparticles and the tertiary amine group in Sar-Na would be responsible for the reduction.[16] Meanwhile, the Au nanoparticles were stabilized by the Sar-Na surfactant to form a suspension. As shown in Scheme 1, the acid in the solution could convert a portion of the Sar anions to Sar-H, which was an amphiphilic polar oil and acted as emulsion droplets. Then the Au nanoparticles stabilized by the surfactant would be hosted and dispersed in the Sar-H polar oil droplets. When the silica precursors of 3-aminopropyltrimethoxysilane (APMS) and TEOS were added to the solution, a silica shell was formed following the $S^{-}N^{+}\sim I^{-}$ pathway, where S stands for a surfactant, N stands for a co-structure directing agent (CSDA), and I stands for inorganic precursors.[17] During the succedent reaction, the initially formed disordered silica/surfactant hybrid mesophases in the shell underwent a structural transformation and finally an ordered shell with radially oriented mesochannels was obtained.[18,19] Finally the rattle structures with mesoporous shells were obtained after the calcination to remove the surfactants. In the process, the Sar-Na surfactant played multiple roles: reducing agent, stabilizer, emulsion droplets after acidification and mesopore template, and by this one-pot method the mesoporous silica hollow spheres with encapsulated Au nanoparticles (Au@MSHS) could be facilely fabricated.

SEM images (Fig. 2a and b) display that the Au@MSHS sample consisted of dispersed spheres. TEM images of Au@MSHS (Fig. 2c and d) show that the particles were hollow spheres, which were intact without aggregation. By measuring the diameter of the particles from the TEM images, it was found that the particle size was mostly in the range of 150–250 nm. It is interesting that all the hollow spheres possess a uniform shell thickness of 25–35 nm independent of their sizes. The significant feature of the hollow spheres was the radially oriented mesochannels in their shells (Fig. 2d and Fig. S3, ESI†) and each silica hollow sphere contained several monodispersed Au nanoparticles inside.

The N_2 adsorption/desorption isotherms of Au@MSHS (Fig. 3a) exhibited a type IV isotherm demonstrating the mesoporous characteristics of the hollow silica spheres.

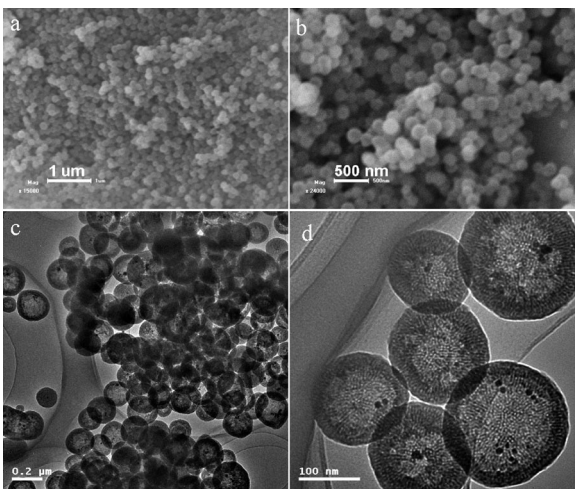

Fig. 2 SEM (a, b) and TEM (c, d) images of Au@MSHS.

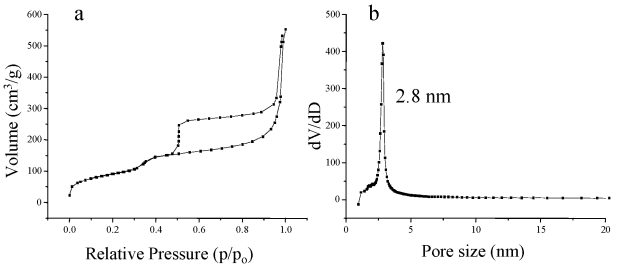

Fig. 3 Nitrogen adsorption–desorption isotherms (a) and the pore size distribution (b) of Au@MSHS.

The adsorption uptake at a relative pressure of 0.95 was attributed to the aggregation voids between the silica nanospheres. The isotherms exhibited a H2 hysteresis loop in the p/p_0 range of 0.5–0.95, which had also been observed for other hollow structures with mesoporous walls, and was ascribed to the delay of nitrogen evaporation from the hollow voids blocked by the surrounding mesopores during the N_2 desorption process.[18,20] The BET surface area, total pore volume and pore size were 330 $m^2\ g^{-1}$, 0.39 $cm^3\ g^{-1}$ and 2.8 nm, respectively (Fig. 3b). The XRD pattern of Au@MSHS displayed diffraction peaks of Au(0) (Fig. S4, ESI†). The UV-vis spectrum (Fig. S5, ESI†) of Au@MSHS displayed an absorption peak at 520 nm, corresponding to excitation of surface plasmon vibrations in the gold nanoparticles.

In the anionic surfactant templated synthesis, the pH value is an important factor to control the self-assembly of the surfactant, co-structure directing agent (APMS) and TEOS.[21] Here in our case, the pH value change would influence the formation of oil droplets, the charge state of APMS and surfactant, as well as the hydrolysis and condensation rate of silica precursors, and it was reasonable that hollow spheres could only be obtained within a certain pH range (Fig. S6–S9, ESI†).

The Sar-Na solution can also be used to reduce other noble precursors, such as H_2PdCl_4. From TEM images (Fig. S10, ESI†), the average size of the Pd nanoparticles in Sar solution was 3.0 nm (with a standard deviation of 0.5 nm). Alloy nanoparticles could also be obtained by this method and different alloy particles could be prepared by altering the order of addition of metal precursors to Sar-Na solution. For instance, Pd–Au alloy nanoparticles were prepared by reducing mixed $HAuCl_4$ and H_2PdCl_4 solution simultaneously (denoted as S-Pd–Au). If H_2PdCl_4 was reduced by Sar solution firstly, and then $HAuCl_4$ was added and reduced again, the alloy was denoted as F-Pd–Au. With swap of the reduction order, an alloy of F-Au–Pd was also prepared. Photographs of alloy nanoparticles in Sar solution and TEM images of alloy nanoparticles are shown in ESI† (Fig. S11–S14). Those three alloy nanoparticles exhibited different shape and size distribution. The fabrication route shown in Scheme 1 could be applied to encapsulate different noble nanoparticles such as Pd, Pt, and their bimetallic alloy nanoparticles into the mesoporous silica hollow spheres. For instance, as shown in Fig. 4, Pd nanoparticles were encapsulated inside silica hollow spheres, and the radially oriented mesopores in the silica shell could be seen. After calcination the Pd nanoparticles were actually oxidized to PdO as shown by the XRD pattern (Fig. S15, ESI†). The N_2

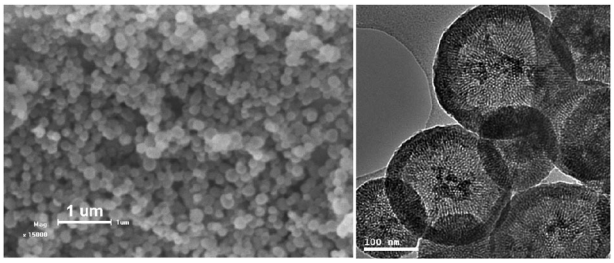

Fig. 4 SEM and TEM images of Pd@MSHS.

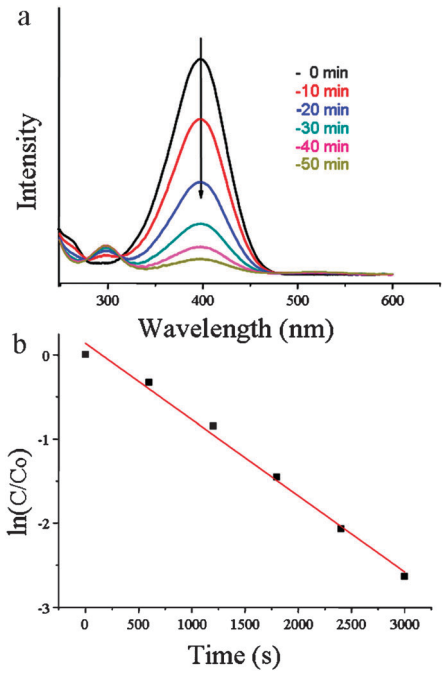

Fig. 5 (a) Time-dependent UV-vis spectral changes of the reaction mixture catalyzed by Au@MSHS. (b) Plot of $\ln(C/C_o)$ *versus* time for Au@MSHS.

adsorption/desorption isotherms of the Pd@MSHS are shown in Fig. S16 (ESI†).

Here, the Au@MSHS (Au weight percent in the catalyst is 0.5 wt%) was tested in catalytic reduction of 4-nitrophenol. The kinetics of 4-nitrophenol reduction in the presence of Au@MSHS was studied by UV-vis spectroscopy. The reaction progress was monitored by taking a small portion of the reaction mixture at a regular time interval. Fig. 5a shows the UV-vis spectra for the reduction of 4-nitrophenol measured at different times during the progress of the reaction. After the addition of Au@MSHS, the peak height at 400 nm decreased and the peak at 300 nm increased gradually with time. A successive decrease of peak intensity at 400 nm with time was taken into consideration to obtain the rate constant. The ratio of C/C_o, where C was the concentration at time t and C_o was the initial concentration, was measured from the relative intensity ratio of the respective absorbance, A/A_o, at 400 nm. The linear relationship of $\ln(C/C_o)$ *versus* time was observed, indicating that the reactions followed first-order kinetics. The observed rate constant for the catalyst was 9.1×10^{-4} s^{-1} calculated directly from the slope of the straight line in Fig. 5b.

In conclusion, we report a facile method for the one-pot fabrication of mesoporous silica hollow spheres with encapsulated noble metal nanoparticles. The green amino acid surfactant Sar-Na serves as the reducing agent, stabilizing agent, polar oil droplets after acidification and mesopore template. This kind of rattle type particles was successfully applied in the catalytic reduction of 4-nitrophenol as a model reaction. In addition, this strategy can be easily extended to fabricate hollow silica nanospheres encapsulating other noble metal nanoparticles, which would be applicable in different aspects.

This work was supported by NSFC (20873070, 20973095 and 81071260), National Basic Research Program of China (2009CB623502), NCET-07-0448 and MOE (IRT-0927).

Notes and references

1 P. Raveendran, J. Fu and S. Wallen, *J. Am. Chem. Soc.*, 2003, **125**, 13940; J. Garcia-Serrano, U. Pal, A. Herrera, P. Salas and C. Angeles-Chavez, *Chem. Mater.*, 2008, **20**, 5146; H. Li, J. Jo, L. Zhang, C. Ha, H. Suh and I. Kim, *Langmuir*, 2010, **26**, 18442; R. Shukla, S. Nune, N. Chanda, K. Katti, S. Mekapothula, R. Kulkarni, W. Welshons, R. Kannan and K. Katti, *Small*, 2008, **4**, 1425; N. Wangoo, K. Bhasin, S. Mehtab and C. Suri, *J. Colloid Interface Sci.*, 2008, **323**, 247; P. Selvakannan, S. Mandal, S. Phadtare, A. Gole, R. Pasricha, S. Adyanthaya and M. Sastry, *J. Colloid Interface Sci.*, 2004, **269**, 97–102; S. Bhargava, J. Booth, S. Agrawal, P. Coloe and G. Kar, *Langmuir*, 2005, **21**, 5949.
2 K. Kamata, Y. Lu and Y. N. Xia, *J. Am. Chem. Soc.*, 2003, **125**, 2384.
3 P. M. Arnal, M. Comotti and F. Schuth, *Angew. Chem., Int. Ed.*, 2006, **45**, 8224.
4 X. W. Lou, L. A. Archer and Z. Yang, *Adv. Mater.*, 2008, **20**, 3987.
5 J. Lee, J. C. Park and H. Song, *Adv. Mater.*, 2008, **20**, 1523.
6 Y. Zhao and L. Jiang, *Adv. Mater.*, 2009, **21**, 3621.
7 W. M. Zhang, J. S. Hu, Y. G. Guo, S. F. Zheng, L. S. Zhong, W. G. Song and L. J. Wan, *Adv. Mater.*, 2008, **20**, 1160.
8 H. X. Li, Z. F. Bian, J. Zhu, D. Q. Zhang, G. S. Li, Y. N. Huo, H. Li and Y. F. Lu, *J. Am. Chem. Soc.*, 2007, **129**, 8406.
9 K. T. Lee, Y. S. Jung and S. M. Oh, *J. Am. Chem. Soc.*, 2003, **125**, 5652.
10 M. Kim, K. Sohn, H. Na and T. Hyeon, *Nano Lett.*, 2002, **2**, 1383; S. Ikeda, S. Ishino, T. Harada, N. Okamoto, T. Sakata, H. Mori, S. Kuwabata, T. Torimoto and M. Matsumura, *Angew. Chem., Int. Ed.*, 2006, **45**, 7063; D. Chen, L. Li, F. Tang and S. Qi, *Adv. Mater.*, 2009, **21**, 3804; W. Choi, H. Koo and D. Kim, *Langmuir*, 2008, **24**, 4633; X. Huang, C. Guo, J. Zuo, N. Zheng and G. Stucky, *Small*, 2009, **5**, 361.
11 J. Lee, J. C. Park, J. Bang and H. Song, *Chem. Mater.*, 2008, **20**, 5839.
12 Q. Zhang, I. Lee, J. P. Ge, F. Zaera and Y. D. Yin, *Adv. Funct. Mater.*, 2010, **20**, 2201.
13 J. H. Gao, G. L. Liang, B. Zhang, Y. Kuang, X. X. Zhang and B. Xu, *J. Am. Chem. Soc.*, 2007, **129**, 1428.
14 X. Wu and D. Xu, *Adv. Mater.*, 2010, **22**, 1516; J. Liu, S. Qiao, S. Hartono and G. Lu, *Angew. Chem., Int. Ed.*, 2010, **49**, 4981.
15 S. Wu, C. Tseng, Y. Lin, C. Lin, Y. Hung and C. Mou, *J. Mater. Chem.*, 2011, **21**, 789.
16 Y. E. Cheon and M. P. Suh, *Angew. Chem., Int. Ed.*, 2009, **48**, 2899.
17 S. Che, A. E. Garcia-Bennett, T. Yokoi, K. Sakamoto, H. Kunieda, O. Terasaki and T. Tatsumi, *Nat. Mater.*, 2003, **2**, 801.
18 J. Wang, Q. Xiao, H. Zhou, P. Sun, D. Ding and T. Chen, *J. Colloid Interface Sci.*, 2008, **323**, 332.
19 J. Wang, F. Li, H. Zhou, P. Sun, D. Ding and T. Chen, *Chem. Mater.*, 2009, **21**, 612.
20 B. Tan, H. J. Lehmler, S. M. Vyas, B. L. Knuston and S. E. Rankin, *Adv. Mater.*, 2005, **17**, 2368.
21 C. Gao and S. Che, *Adv. Funct. Mater.*, 2010, **20**, 2750.

